Article

Glycine–Nitrate Combustion Synthesis and Photocatalytic Degradation Properties of Cu-Based Nanoparticles

Hsu-Hui Cheng[1*], Shiao-Shing Chen[2*], Liang-Wei Jang[2], Hui-Ming Liu[3]

[1] School of Environmental and Chemical Engineering, Zhaoqing University, Zhaoqing, 526061, China; hhcheng1126@gmail.com (H.-H. Cheng)
[2] Institute of Environment Engineering and Management, National Taipei University of Technology, 1, Sec.3 Chung-Hsiao E. Rd., Taipei 10643, Taiwan; f10919@ntut.edu.tw (S.-S. Chen)
[3] Department of Safety, Health and Environmental Engineering, Hungkuang University, Taichung 43302, Taiwan; hmliu@sunrise.hk.edu.tw (H-M. Liu)
* Correspondence: hhcheng1126@gmail.com (H.-H. Cheng); f10919@ntut.edu.tw(S.-S. Chen); Tel.: +86-19867382107 (H.-H. Cheng)

Abstract: Copper-based nanoparticles were synthesized using the glycine–nitrate process (GNP) by using copper nitrate trihydrate [$Cu(NO_3)_2 \cdot 3H_2O$] as the main starting material and glycine [$C_2H_5NO_2$] as the complexing and incendiary agent. The as-prepared powders were characterized through X-ray diffraction (XRD), Brunauer–Emmett–Teller (BET) analysis, X-ray photoelectron spectroscopy, and scanning electron microscopy. Using $Cu(NO_3)_2.3H_2O$ as the oxidizer (N) and glycine as fuel (G), we obtained CuO, mixed-valence copper oxides (CuO + Cu_2O, G/N = 0.3–0.5), and metallic Cu (G/N = 0.7). The XRD and BET results indicated that increasing the glycine concentration (G/N = 0.7) and reducing particle surface area increased the yield of metallic Cu. The effects of varying reaction parameters such as catalyst activity, catalyst dose, and H_2O_2 concentration on nonylphenol-9-polyethoxylate (NP9EO) degradation were assessed. With a copper-based catalyst in a heterogeneous system, the NP9EO and total organic carbon removal efficiencies were 83.1% and 70.6%, respectively, under optimum operating conditions (pH, 6.0; catalyst dose, 0.3 g/L; H_2O_2 concentration, 0.05 mM). The results suggested that removal efficiency increased with an increase in H_2O_2 concentration but decreased when the H_2O_2 concentration exceeded 0.0.5 mM. Furthermore, the trend of photocatalytic activity was as follows: G/N = 0.5 > G/N = 0.7 > G/N = 0.3. The G/N = 0.5 catalysts showed the highest photocatalytic activity and resulted in 94.6% NP9EO degradation in 600 min.

Keywords: glycine-nitrate process; copper oxide nanopowders; heterogeneous catalysis; NP9EO

1. Introduction

Combustion synthesis is an effective, simple, and rapid process, which is used for efficient synthesis of various catalytic nanomaterials [1]. Recently, several novel procedures and modifications of combustion synthesis have been used to obtain ceramic nanomaterials with desired properties for different applications. The glycine–nitrate process (GNP) has been frequently employed for preparing complex nanostructured metal oxides or catalytic nanomaterials [2-4]. The GNP is highly suitable for synthesizing fine crystalline powders and nanometer-scale particles with desirable characteristics such as high chemical homogeneity, high purity, and a narrow size distribution range of powder particles [5]. The GNP is a type of solution combustion synthesis, which involves a self-sustained reaction between an oxidizer, such as a metal nitrate solution, and a fuel such as glycine [4,6,7]. Furthermore, glycine supplies the energy required for combustion and acts as a complexing agent. An advantage of the GNP is that the rapid evolution of a large volume

of gaseous products during combustion dissipates the heat of the process and limits the increase in temperature, which reduces the probability of local sintering among catalyst particles while simultaneously facilitating the formation of a fine powder [5].

In recent years, nanosized particles of transition metal oxides (TMO) have attracted considerable attention because of their unique applications in various fields, such as chemicals, catalysts [4,8], photocatalysts [9], solar cells [4], and gas sensors [10]. Preparation of high-quality nanostructures with a defined and controllable size and morphology is the main determinant of the catalytic performance [11]. Among nanocatalysts, TMO-based catalysts offer active sites with low activation potential for hydrogen-evolution systems [10]; in particular, noble metals (such as gold, silver, and platinum) have been widely used to optimize catalytic efficiency. However, the high cost of noble metals remains a major obstacle in developing stable and highly efficient catalysts. Consequently, reducing the amount of noble metals without compromising on their catalytic performance is an urgent requirement in catalysis.

Compared with noble metal catalysts, copper, which is inexpensive, moderately abundant, and safe, has recently drawn scientific attention as a cocatalyst in photoreforming processes [12]. Copper oxides (Cu_xO_y, where x:y = 1:1 or 1:2) and metallic copper are widely used as TMO catalysts. Copper oxides are heterogeneous catalysts with high recyclability, high catalytic efficiency, and low bandgap energies [11]. Cu oxides (Cu_xO_y, where x:y = 1:1 or 1:2) are used as TMO catalysts; Cu_xO_y catalysts are p-type semiconductors with a monoclinic structure, a bandgap of 1.7–2.17 eV [14], and a high theoretical photocurrent density of −14.7 mA/cm^2 [13-15]; therefore, they are suitable for application in catalysis. However, in all applications of Cu_xO_y morphology, size, and surface area are the main determinants of catalytic performance [15]. Compared with other TMOs, such as titanium dioxide (TiO_2), zinc oxide (ZnO), iron oxide (Fe_2O_3), and cadmium sulfide (CdS), only a few studies have described synthesis strategies for different Cu_xO_y nanoparticles along with the introduction of their related applications.

In this study, we present a low-temperature GNP with varying G/N ratios for synthesizing Cu_xO_y and metallic copper catalysts. Furthermore, the degradation of nonylphenol-9-polyethoxylate (NP9EO) under ultraviolet (UV) irradiation by using a heterogeneous copper oxide catalyst (and metallic copper) in a custom-made photoreactor was investigated. Moreover, the effects of operational parameters, such as the catalyst activity, dose, and solution pH, were examined.

2. Materials and Methods

2.1. Catalyst Preparation

To synthesize Cu-based materials by using the GNP, copper nitrate trihydrate [$Cu(NO_3)_2 \cdot 3H_2O$] (Merck, USA, 99.5% purity) and glycine [$C_2H_5NO_2$] (Merck, USA, 99.7% purity) were dissolved in distilled water. Varying amounts of glycine (fuel) were added to the metal nitrate (oxidizer) solution to obtain different glycine–nitrate (G/N) ratios (G/N = 0.3, 0.5, and 0.7). As shown in Figure 1, the glycine–nitrate solutions were then mixed and heated overnight over a hot-plate stirrer (Corning, USA) at 105°C to form clear, homogeneous, and viscous gel-like solutions. Each gel was then poured into a ceramic bowl that was placed in an oven. The gels were heated to 200°C until they underwent self-ignition and produced catalyst ash.

2.2. *Characterization*

The crystal structure of the samples was determined through powder X-ray diffraction (XRD) by using Cu Kα radiation (λ = 1.5418 Å) on a Rigaku DMAX 2200VK/PC diffractometer (Tokyo, Japan). All peaks measured using XRD were assigned by comparison with those of data from the Joint Committee on Powder Diffraction Standards (JCPDS) [16]. The chemical composition of the samples was verified using X-ray photoelectron spectroscopy (XPS; VG Escalab 250 iXL) for chemical analysis. The specific surface area ($m^2\ g^{-1}$) was calculated using the Brunauer–Emmett–Teller (BET) equation, and total pore volume (Vt, $m^3\ g^{-1}$) was evaluated by converting the adsorption amount at P/P0 = 0.95 to the volume of the liquid adsorbate. The morphologies of the synthesized samples were analyzed through scanning electron microscopy (SEM, Hitachi S-4800) coupled with energy dispersive X-ray spectroscopy (EDS) measurements.

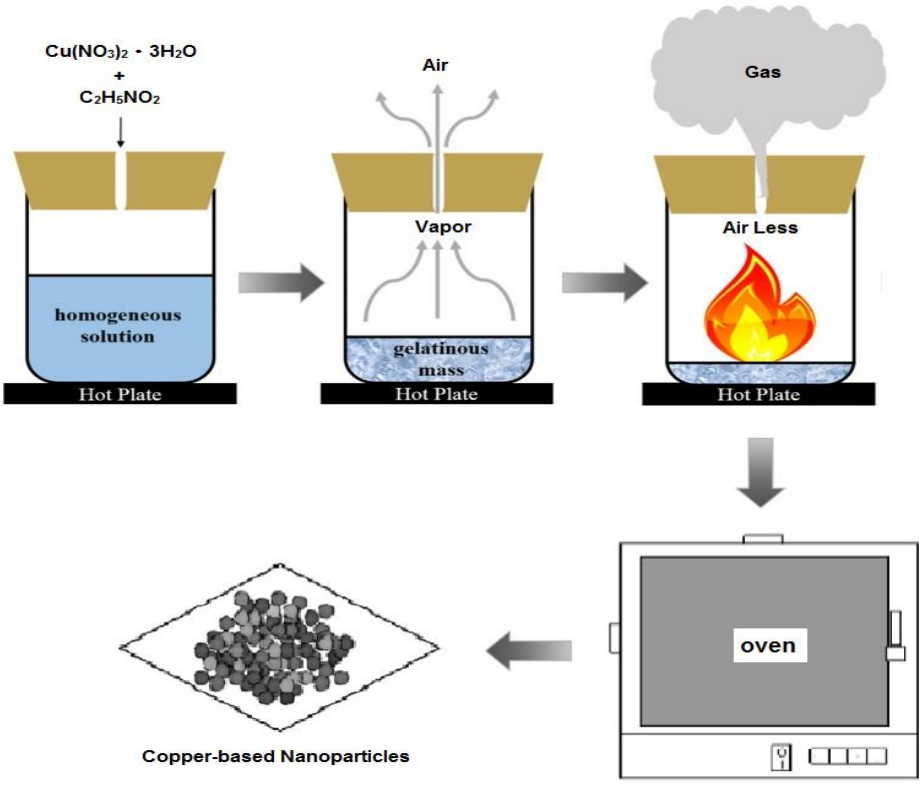

Figure 1. Schematic illustration of combustion synthesis for the copper nitrate–glycine reaction system.

2.3. *Photocatalytic experiments*

NP9EO (reagent grade) with an average of 9 ethylene oxide units (Sigma-Aldrich, USA, purity ≥ 99.7%) was selected as a model compound for analysis; its chemical structure is shown in Figure 2. The stock solutions of NP9EO were prepared in distilled water to obtain a concentration of 100 mg/L, which was then ultrasonicated for 30 min to obtain a stable emulsion. The emulsion was stored at 4°C for a maximum of 4 weeks. The photocatalytic reaction was conducted in a custom-made photoreactor (Panchum Scientific Co., PR-2000), as illustrated in Figure 3. The photocatalytic activities of nano-Cu samples under UV irradiation were evaluated based on the degradation rate of NP9EO in a quartz reactor (120/115 mm outer/inner diameter, height: 240 mm) containing 0.3 g of nano-Cu (G/N = 0.3) and 1 L of a 100 mg/L aqueous solution of NP9EO. The system was open to the

atmosphere, and the cylindrical quartz reactor was surrounded by a total of 14 light tubes. The UV light tubes were germicidal lamps with a wavelength of 254 nm (Sankyo Denki Co., Ltd.). The light power (approximately 10 mW/cm^2) in the center of the reactor in air was measured using a power meter (Model 840-C Handheld). The photodegradation rate of NP9EO solution was determined through high-performance liquid chromatography (Agilent 1100 series; Agilent Technologies, USA) with Wondasil-C18 (4.6 × 150 mm, 5 μm), and a 2487-UV detector at 277 nm.

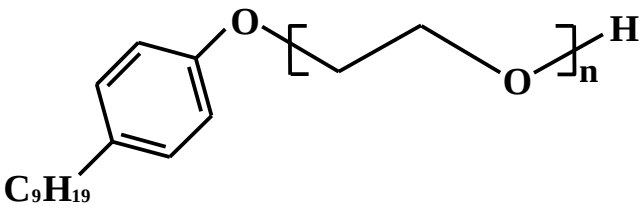

Figure 2. Chemical structure of NPnEO

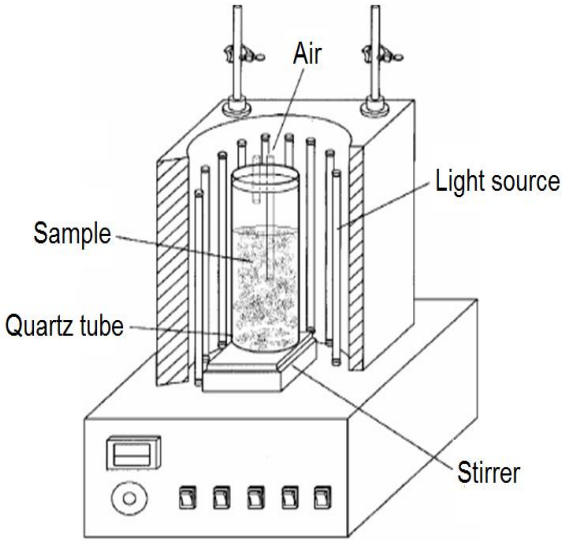

Figure 3. Schematic representation of the custom-made photoreactor

3. Results and Discussion

3.1. *Characterization of Cu-Based nanoparticles catalyst*

Figure 4 depicts the XRD pattern of as-synthesized copper-based nanoparticles synthesized using the GNP method by using different G/N ratios. At a stoichiometric G/N ratio of 0.5 (see sample (b) in Figure 4), intense reflections were observed at 2θ values of 29.5°, 36.8°, 38.7°, 42.3°, 43.4°, 50.5°, 61.4°, and 74.2°. The peaks at 38.7° corresponded to the (111) plane of divalent copper (II) oxide (CuO), whereas the reflections at 29.5°, 36.8°, 42.3° and 61.4°corresponded to the (110), (111), (200), and (220) planes of cuprite, respectively (JCPDS File No. 01-078-0428), which indicated the formation of cubic copper (I) oxide (Cu_2O) nanocrystals (JCPDS File No. 01-077-0199). In addition, peaks at 50.5° and 74.2°, which corresponded to the (200) and (220) peaks, respectively, of zero-valent copper (Cu^0) were observed. These results clearly illustrated that Cu^0 nanoparticles formed in the chemical reduction stage underwent decomposition because of limited stability of Cu

[17,19], and Cu_2O might be formed by oxidation [18-19]. When the G/N ratio increased to 0.7, broad reflections because of a highly dispersed Cu^0 phase were observed in sample (c) in Figure 1. The XRD patterns (111), (200), and (220) of Cu^0 planes at 43.4°, 50.5°, and 74.2°, respectively, were consistent with bulk copper crystallographic data (JCPDS File No. 01-085-1326). The results clearly showed that the formation of Cu^0 was favored with an increase in glycine (fuel) content in combustion synthesis [1]. When the G/N ratio was reduced to 0.3, the sample (a) exhibited numerous primary CuO phases and a few Cu_2O phases (about 9.5%). These findings indicated that the nanocrystalline CuO was reduced to a stable Cu_2O phase rather than forming metallic copper directly [20].

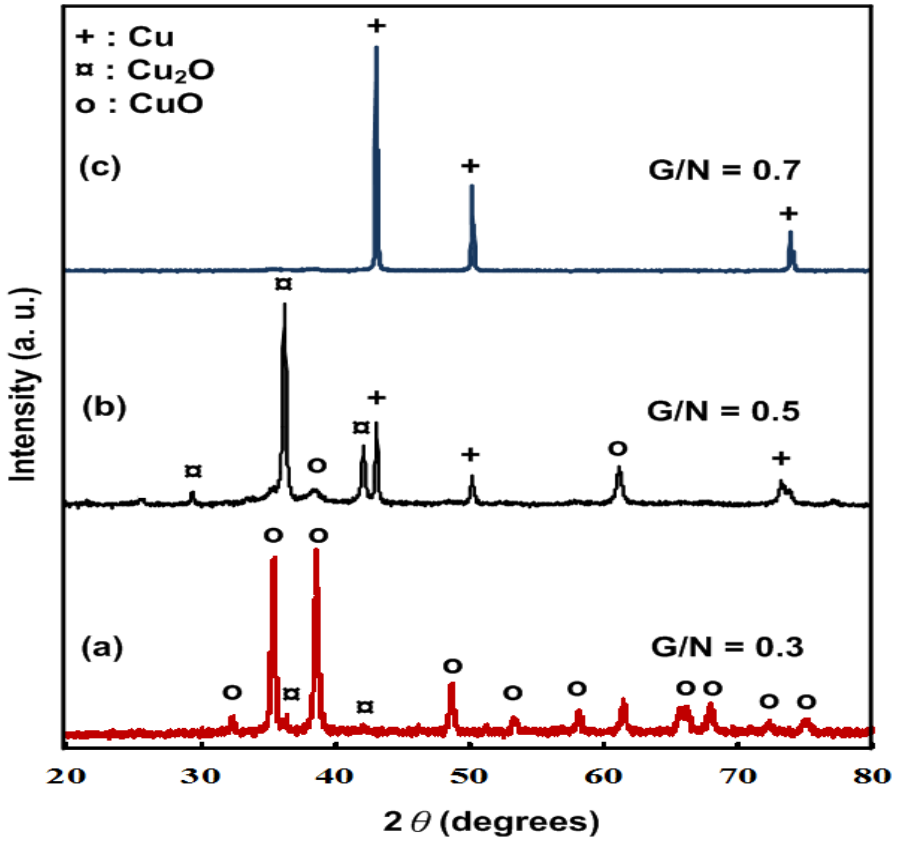

Figure 4. The XRD pattern of combustion synthesized products of copper-based materials with various glycine-nitrate ratio (G/N) = 0.3(a), 0.5(b), and 0.7(c).

Figure 5 shows the SEM with EDS images of as-prepared Cu-based nanoparticles at various G/N ratios. The typical EDS spectra of the particles (Figure 5) indicated that the particles were composed of copper (Cu) and oxygen (O). The SEM photographs showed that the catalysts formed sponge-like aggregates containing some nanoparticles; the size distribution range of the synthesized particles was broad (5–100 nm), and some irregular granules with a high degree of shape anisotropy were observed. The prepared Cu-based nanoparticles were not single-domain particles. The lack of homogeneity in particle shape and size as well as the presence of sponges or flake-like structures was typical of combustion synthesis. The results indicated that the large

amounts of gas evolved during combustion affected the porosity of solid products [21,22]. Moreover, high combustion temperatures promoted nanoparticle agglomeration and crystal grain growth [23]. This finding was consistent with the surface area (BET) analysis results in the present study (Table 1). The BET results indicated that increasing the glycine concentration and reducing particle surface area promoted the formation of metallic Cu. Consequently, large-scale agglomerates were observed when the ratio G/N = 0.7 was used.

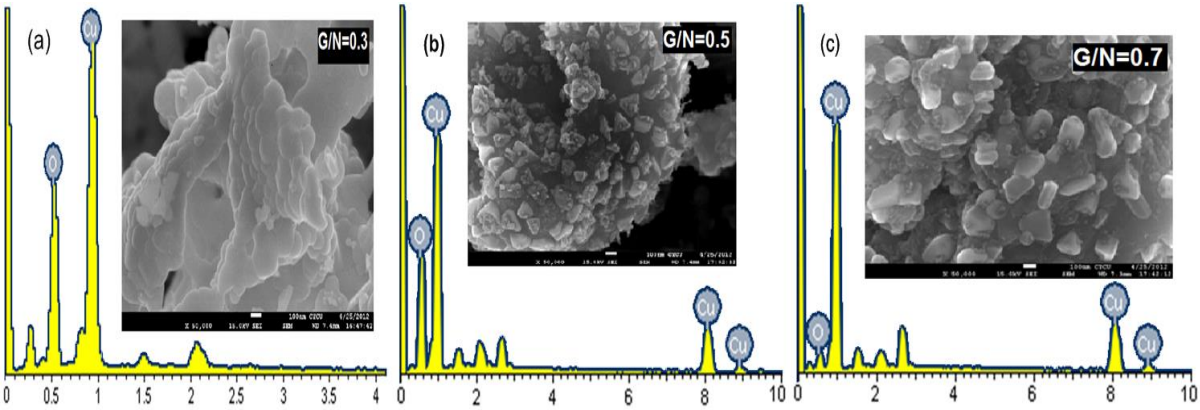

Figure 5. SEM with EDS images of prepared Cu-based nanoparticles at various G/N ratios: G/N = 0.3 (a), G/N = 0.5 (b), and G/N = 0.7 (c).

Table 1. Specific surface area and determination of copper oxide nanoparticles synthesized at different G/N ratios

Catalyst	Synthesis of copper oxide nanoparticles ratio analysis [%]			Specific surface area [m^2/g]
	CuO	Cu_2O	Cu	
G/N=0.3	90.5	9.5	0	166.922
G/N=0.5	43.2	54.6	2.2	131.039
G/N=0.7	0	24.8	75.2	92.134

X-ray photoelectron spectroscopy (XPS) spectra of the selected catalysts were obtained to confirm the surface composition and oxidation state of copper, based on information derived from the values of binding energies. Copper oxidation states existed in two semiconducting phases, namely cupric oxide (CuO) and cuprous oxide (Cu_2O) [24]. The binding energies in the XPS analysis were calibrated using C 1s peak (BE = 284.6 eV), where the C 1s peak was attributed to residual carbon from the sample and adventitious hydrocarbons from the XPS instrument itself or adsorbed carbon. Figure 6 shows the three samples obtained from XPS results. As shown in Figure 6 (a), the main O 1s peak present at 532.8 eV was attributed to lattice oxygen in a metal oxide, such as CuO or Cu_2O. The Cu 2p3/2 XPS core level spectra of copper oxides are shown in Figure 6 (b) to (d). In the Cu 2p3/2 core level XPS region, we observed that the binding energies of Cu_2O and CuO were in the ranges 933.1–933.7 eV and 934.3–934.5 eV for different samples, respectively [25,26].

Additionally, two peaks were observed, and the feature at 932.4 ± 0.1 eV was attributed to metallic Cu (2p3/2) [25,26], as shown in Figure 6 (c) and (d) respectively.

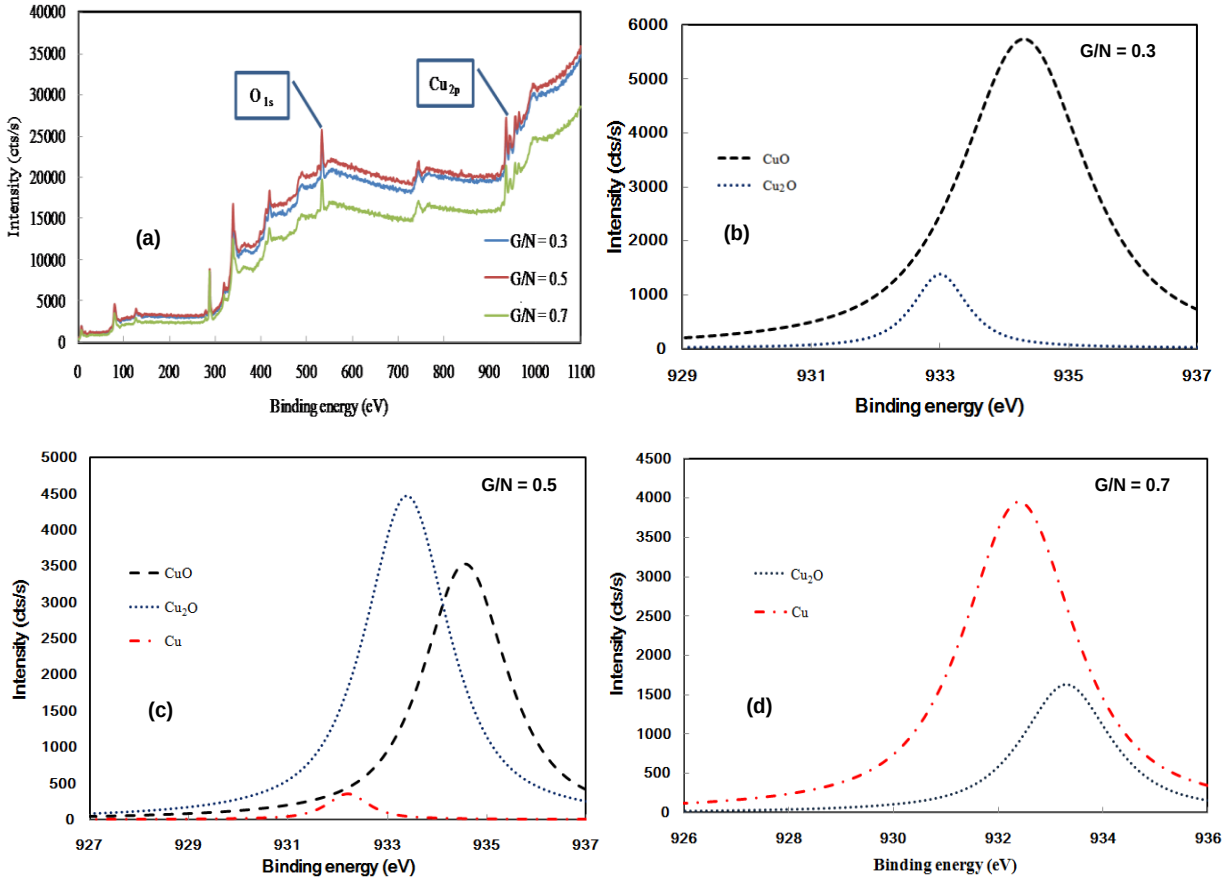

Figure 6. XPS wide-scan spectrum (a) of all samples; XPS spectra of (b) (G/N) = 0.3, (c) (G/N) = 0.5, and (d) (G/N) = 0.7 of all samples.

3.2 Evaluation of Photocatalytic Performance

The degradation of NP9EO was used in this study to evaluate the photocatalytic activity of the as-prepared samples. Catalyst dose is one of the main parameters in degradation studies from an economical point of view. For optimizing the dose of nano-Cu catalysts, experiments were performed by varying nano-Cu (G/N = 0.3) dose from 0.1 to 1 g/L. Figure 7(a) shows that the degradation efficiencies for 0.1, 0.3, 0.5, 0.8, and 1.0 g/L nano-Cu (G/N = 0.3) were 80.1%, 83.1%, 78.2%, 73.6%, and 70.3%, respectively. Therefore, the optimal dose of nano-Cu catalysts (G/N = 0.3) in this custom-made photoreactor was 0.3 g/L.

Additionally, the effect of H_2O_2 concentration (0–0.1 M) on photocatalytic oxidation was investigated. The experimental results showed that removal efficiency increased with an increase in H_2O_2 dosage. When the dose of H_2O_2 was increased to 0.05 mM, the highest NP9EO and TOC removal efficiencies were obtained, namely 83.1% and 70.6%, respectively. Subsequently, the NP9EO and TOC removal efficiencies exhibited a gradual decrease with an increase in H_2O_2 dose (shown in Figure 7 (b)). This finding can be explained. At low H_2O_2 doses, an increase in H_2O_2 dose

increased the concentration of hydroxyl radicals (OH •) [27], which was conducive to the degradation of NP9EO. However, when the dose of H_2O_2 exceeded 0.05 mM (higher doses), H_2O_2 started inhibiting the destruction of the NP9EO, which is thought to be due to the reaction between excess H_2O_2 and OH • radicals (Reactions (1) and (2)), thereby reducing the amount of OH • available for reaction with NP9EO [28-29].

$$H_2O_2 + OH\bullet \rightarrow HO_2\bullet + H_2O \quad (1)$$

$$HO_2\bullet + HO_2\bullet \rightarrow O_2 + H_2O \quad (2)$$

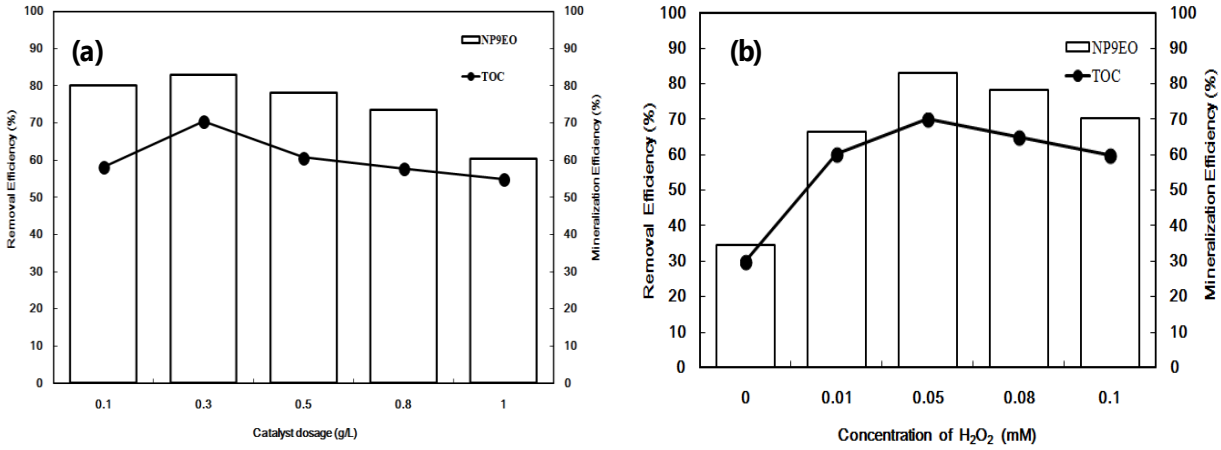

Figure 7. (a) Effect of catalyst dose on the degradation of NP9EO (Catalyst G/N = 0.3, NP9EO = 100 mg/L, H_2O_2 = 0.05 mM (1000 mg/L), pH = 6), (b) Effect of increasing H_2O_2 concentration on NP9EO degradation. (Catalyst G/N = 0.3, NP9EO =100 mg/L, pH = 6, catalyst dosage = 0.3g/L)

The effect of different G/N ratios of Cu-based nanoparticles on photocatalytic activity was also investigated in this study (Figure 8). The order of photocatalytic activity was as follows: G/N = 0.5 > G/N = 0.7 > G/N = 0.3. The G/N = 0.5 catalysts showed the highest photocatalytic activity and resulted in 94.6% NP9EO degradation and 70.5% TOC reduction after 600 min. These results clearly suggested that at G/N = 0.5, the catalyst exhibited a high activity, which was represented as the degradation of NP9EO. This finding is consistent with the results of XPS analysis of the oxidation state of copper (see the Table 1). Cu_2O (bandgap of approximately 2.2 eV) has higher electric conductivity than CuO (bandgap of approximately 1.6 eV) [30]; therefore, Cu_2O exhibits a higher removal effect than CuO in a photocatalytic system. Furthermore, Cu_2O and CuO are more stable at a higher potential for photoelectrochemical/hydrogen-evolution reaction because a high potential restrains the photoreduction of Cu_2O (or CuO) to metallic copper [31]. Dasineh et al. [30] reported that the integration of Cu_2O and CuO significantly increased charge collection and reduced the recombination rate inside the photocatalyst. Cu_2O and CuO improved optical absorption and facilitated charge transfer at the interface between the photocatalyst and electrolyte. Consequently, with copper-based catalysts in a heterogeneous system, the highest photocatalytic performance was obtained with a G/N ratio of 0.5. Furthermore, in our results, the efficiency of NP9EO removal was

consistently lower than that of TOC removal, indicating that in addition to CO_2 (formed by mineralization), some intermediates were generated (such as by-products) [32]. The main reason for NP9EO cannot, therefore, be effectively mineralized.

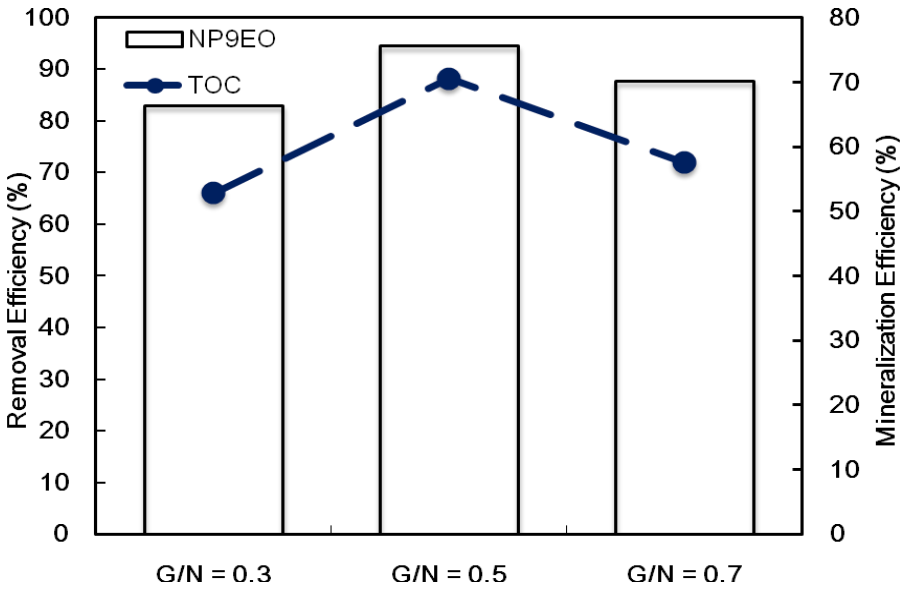

Figure 8. NP9EO degradation curves for Cu-based catalysts synthesized at different G/N ratios (Catalyst dosage = 0.3g/L, NP9EO =100 mg/L, H_2O_2 = 0.05 mM (1000 mg/L), pH = 6,)

4. Conclusions

A nanocrystalline Cu-based heterogeneous catalyst was successfully synthesized using the GNP. The nature and amount of fuel were crucial factors in controlling the combustion process and final product composition. The formation of CuO, mixed-valence copper oxides (CuO+Cu_2O),and metallic Cu was achieved by varying the G/N ratio, where glycine was used as a fuel. The effect of the G/N ratio on the morphology of the catalysts was analyzed using SEM. When a G/N ratio of 0.7 was used, the formation of agglomerate structures was observed. Furthermore, Cu-based catalysts exhibited high photocatalytic activity during the degradation of NP9EO in a custom-made photoreactor under UV light. The experimental results revealed that under optimal reaction conditions, namely catalyst dose of 0.3 g/L and H_2O_2 concentration of 0.05 mM, NP9EO and TOC removal efficiencies were 83.1% and 70.6%, respectively. The removal efficiency increased with H_2O_2 concentration, but decreased when the H_2O_2 concentration exceeded 0.05 mM. With the Cu-based catalysts in a heterogeneous system, the highest photocatalytic activity was observed at a G/N ratio of 0.5, which resulted in 94.6% NP9EO degradation and 70.5% TOC reduction after 600 min.

Author Contributions: S.S.-C. and H.H.-C. conceived and designed the experiments; L.W. -J. performed the experiments; L.W. -J. analyzed the data; S.S.-C. Project administration; H.H.-C. Writing—review & editing; H.M. -L. review. The manuscript was revised through the comments of all authors. All authors have approved the final version of the manuscript.

Funding: This study was supported by grant from Hsuteng Consulting International Co., Ltd.

Acknowledgments: The authors gratefully acknowledge experimental apparatus support from Institute of Environment Engineering and Management, National Taipei University of Technology.

Conflicts of Interest: The authors declare no conflict of interest.

References

1. Rao, G.R.; Mishra, B.G.; Sahu, H.R. Synthesis of CuO, Cu and CuNi alloy particles by solution combustion using carbohydrazide and N-tertiarybutoxy-carbonylpiperazine fuels. *Mater. Lett.* **2004**, *58*, 3523-3527.
2. Wan, L.; Cheng, J.G.; Fan, Y.M.; Liu,Y.; Zheng, Z.J. Preparation and properties of superfine W–20Cu powders by a novel chemical method. *Mater. Des.* **2013**, *51*, 136-140.
3. Coutinho, J.P.; Silva, M.C.; Meneghetti, S.M.P.; Leal, E.; de Melo Costa, A.C.F.; de Freitas, N.L. Combustion synthesis of $ZnAl_2O_4$ catalyst using glycine as fuel for the esterification and transesterification of soybean oil: influence the form of heating. *Mater. Sci. Forum.* **2012**, *727-728*, 1323-1328.
4. Lim, H.H.; Chua, P.N.; Mun, H.P.; Horri, B.A. Synthesis and characterisation of CuO/HNT nano-particles through in-situ glycine nitrate process. *Int. J. Adv. Sci .Eng. Inf. Technol.* **2018**, *6*, 2321-8991.
5. Tajuddin, M.M.; Patulla, M.H.; Ideris, A.; Ismail, M. Self-combustion synthesis of Ni catalysts modified with La and Ce using Glycine–NitrateProcess (GNP). *Malay. J. Catal.* **2017**, *2*, 8-11.
6. Jadhav, L.D.; Patil, S.P.; Chavan, A.U.; Jamale, A.P.; Puri, V.R. Solution combustion synthesis of Cu nanoparticles: a role of oxidant-to-fuel ratio. *Micro.Nano.Lett.* **2011**, *6*, 812-815.
7. Chick, L.A.; Pederson, L.R.; Maupin, G.D.; Bates, J.L.; Thomas, L.E.; Exarhos, G.J. Glycine-nitrate combustion synthesis of oxide ceramic powders. *Mater. Lett.* **1990**, *10*, 6-12.
8. Laguna-Marco, M.A.; Haskel, D.; Souza-Neto, N.; Lang, J.C.; Krishnamurthy, V.V.; Chikara, S.; Cao, G.; van Veenendaal, M. Orbital magnetism and spin-orbit effects in the electronic structure of $BaIrO_3$. *Phys. Rev. Lett.* **2010**, *105*, 216407-1-4.
9. Jiao, F.; Frei, H. Nanostructured cobalt and manganese oxide clusters as efficient water oxidation catalysts. *Energy Environ. Sci.* **2010**, *3*, 1018-1027.
10. Li, W. Y.; Xu, L. N.; Chen, J. Co_3O_4 nanomaterials in lithium-ion batteries and gas sensors. *Adv. Funct. Mater.* **2005**, *15*, 851-857.
11. Tran, T. H.; Nguyen, V. T. Copper oxide nanomaterials prepared by solution methods, some properties, and potential applications: a brief review. *Int. Sch. Res. Notices.* **2014**, *2014*, 1-14.
12. Clarizia, L.; Spasiano, D.; Di Somma, I.; Marotta, R.; Andreozzi, R.; Dionysiou, D.D. Copper modified-TiO_2 catalysts for hydrogen generation through photoreforming of organics. A short review. *Int. J. Hydrogen Energy* **2014**, *39*, 16812-16831.
13. Bandara, J.; Udawatta, C. P. K.; Rajapakse, C. S. K. Highly stable CuO incorporated TiO_2 catalyst for photocatalytic hydrogen production from H_2O. *Photochem. Photobiol. Sci.* **2005**, *4*, 857-861.
14. Janczarek, M.; Kowalska, E. On the origin of enhanced photocatalytic activity of copper-modified titania in the oxidative reaction systems. *Catal.* **2017**, 7, 317-342.
15. Abd-Elkader, O.H.; Deraz, N. Synthesis and characterization of new copper based nanocomposite. *Int. J. Adv. Sci .Eng. Int. J. Electrochem. Sci.* **2013**, *8*, 8614-8622.

16. Sarkar, D. K.; Paynter, R. W. One-step deposition process to obtain nanostructured superhydrophobic thin films by galvanic exchange reactions. *J. Adhes. Sci. Technol.* **2013**, *24*,1181-1189.
17. Aslam, M.; Gopakumar, G.; Shoba, T.L.; Mulla, I.S.; Vijayamohanan, K.; Kulkarni, S.K.; Urban, J.; Vogel, W. Formation of Cu and Cu_2O nanoparticles by variation of the surface ligand: preparation, structure, and insulating-to-metallic transition. *J. Coll. Interf. Sci.* **2002**, *255*, 79-90.
18. Feng, L.; Zhang, C.; Gao, G.; Cui, D. Facile synthesis of hollow Cu_2O octahedral and spherical nanocrystals and their morphology-dependent photocatalytic properties. *Nanoscale Res. Lett.* **2012**, *7*, 276-286.
19. Khan, A.; Rashid, A.; Younas, R.; Chong, R. A chemical reduction approach to the synthesis of copper nanoparticles. *Int. Nano Lett.* **2016**, *6*, 21-26.
20. Pike, J.; Chan, S. W.; Zhang, F.; Wang, X. Formation of stable Cu_2O from reduction of CuO nanoparticles *Appl. Catal. A-Gen.* **2006**, *303*, 273-277
21. Patil, K.C.; Hegde, M.S.; Rattan, T.; Aruna, S.T. Chemistru of nanocrystalline oxide materials: combustion synthesis, properties and applications, *World Scientific Publishing Co. Pte. Ltd.* 2008, Singapore.
22. Kumar, A.; Cross, A.; Manukyan, K.; Bhosale, R.R.; van den Broeke, L.J.P.; Miller, J.T.; Mukasyan, A.S.; Wolf, E.E. Combustion synthesis of copper–nickel catalysts for hydrogen production from ethanol. *Chem. Eng. J.* **2015,** *278*, 46–54.
23. Podbolotova, K. B.; Khorta, A. A.; Tarasovb, A. B.; Trusovc, d, G. V.; Roslyakovd, d, S. I.; Mukasyan, A. S. Solution combustion synthesis of copper nanopowders: the fuel effect. *Combust. Sci. Technol.* **2017**, *189*, 1878-1890.
24. Korzhavyi, P. A.; Johansson, B. Literature review on the properties of cuprous oxide Cu_2O and the process of copper oxidation. SKB Report TR-11-08, Swedish Nuclear Fuel and Waste Management Company, 2011.
25. Biesinger, M. C. Advanced analysis of copper X-ray photoelectron spectra. *Surf. Interface Anal.* **2017**, 49, 1325–1334.
26. Monte, M.; Munuera, G.; Costa, D.; Conesa, J. C.; Martínez-Arias, A. Near-ambient XPS characterization of interfacial copper species in ceria-supported copper catalysts. *Phys. Chem. Chem. Phys.* **2015**, *17*, 29995-30004.
27. Zhang, L.; Wang, L.; Liu, P.; Fu B.; Hwang, J.; Chen, S. Analysis on deep treatment effect of coking wastewater using 3D electrode combined with Fenton reagent. *Charact. Mater. Met. Mater.* 2015, 185–192
28. Nezamzadeh-Ejhieh, A.; Salimi, Z. Heterogeneous photodegradation catalysis of o-phenylenediamine using CuO/X zeolite. *Appl. Catal. A: Gen.* **2010**, *390*, 110–118.
29. Inchaurrondo, N.; Cechini, J.; Font, J.; Haure, P. Strategies for enhanced CWPO of phenol solutions. *Appl. Catal. B: Environ.* **2012**, *111-112*, 641–648.
30. Dasineh Khiavi, N.; Katal, R.; Kholghi Eshkalak, S.; Masudy-Panah, S.; Ramakrishna, S.; Jiangyong, H. Visible light driven heterojunction photocatalyst of CuO-Cu_2O thin films for photocatalytic degradation of organic pollutants. *Nanomaterials.* **2019**, *9*, 1011-1022.
31. Yang, Y.; Xu, D.; Wu, Q.; Diao, P. Cu_2O/CuO Bilayered Composite as a high-efficiency photocathode for photoelectrochemical hydrogen evolution reaction. *Sci. Rep.* **2016**, *6*, 1-13.

32. Chen, S. S.; Hsu, H. T.; Tsui, H. J.; Chang, Y. M. Removal of nonionic surfactant from electroplating wastewater by fluidized zerovalent iron with two oxidants (H_2O_2/$Na_2S_2O_8$). *Desalination Water Treat.* **2013**, *51*, 1678–1684.